Energy Scheduling for Industries under Real-Time Tariffs: Effects of On-Site PV and Battery Storage

Mohamed Ali Hadj Taieb Author, Jaineel Desai Author, Alexander Bade Author, Jessica Rövekamp Author

Hochschule Albstadt-Sigmaringen, Marie-Curie-Straße 22, 72488 Sigmaringen, +49 (0) 7571 732-8311, hadjtaieb@hs-albsig.de, www.hs-albsig.de

Abstract: Industrial manufacturing is electricity-intensive and increasingly exposed to time-varying electricity prices and decarbonization pressure. Energy-aware production scheduling combined with on-site photovoltaics (PV) and battery storage systems (BSS) offers a promising pathway to reduce costs and emissions while enabling market-based flexibility. This paper presents a scheduling framework that jointly optimizes industrial production, PV generation, and BSS operation under realistic plant constraints, including shift plans, operating modes, labor and facility costs. The framework generates a baseline production schedule and a set of Alternative Production Plans (APPs) suitable for selection and coordination within a cluster of industrial facilities, each associated with activation costs. The approach is validated using real industrial data over multiple 7-day horizons across seasons, production volumes, and a range of BSS sizes. Performance is assessed using three key performance indicators: average daily energy-cost reduction, CO_2 impact based on hourly grid emission factors, and average daily offered flexibility. Results from a use case show that price-aware scheduling alone yields substantial cost savings, while BSS acts as a flexibility multiplier, significantly increasing offered flexibility under favorable PV and price conditions. However, storage benefits are highly seasonal and non-linear with size, and cost-optimal operation does not necessarily imply emission optimal outcomes. The proposed framework provides a realistic and scalable basis for evaluating industrial flexibility, PV/BSS sizing, and market participation strategies under real-time tariffs.

Keywords: Industrial demand response, Energy flexibility, Energy-aware production scheduling, Continuous-process manufacturing, PV generation, Battery storage systems.

1 Introduction

Manufacturing is electricity-intensive and central to global energy demand. The sector accounts for around 30% of world's total energy use [1], and global industrial energy consumption is projected to increase by 50% by 2050 [2]. About 24% of global GHG emissions come from industrial energy use and roughly 5% from industrial processes [3], which puts sustained pressure on manufacturers to cut costs and emissions without compromising the industry output [4].

Two main levers dominate current industrial decarbonization efforts. First, energy-aware production scheduling exploits time-varying tariffs such as Time-of-Use (TOU) and Real-Time Pricing (RTP) to shift energy-intensive tasks to lower-price hours while maintaining throughput [5]. Second, on-site resources, notably PV and BSS, reduce grid dependency and buffer PV variability through storage charge and discharge arbitrage [6] [7]. Concrete deployments, however, must respect operational constraints, including shift plans, production-line operating

states, labor and facility costs, and explicit PV/BSS grid power balances. While literature reports consistent savings under TOU pricing and growing interest in RTP [8], many studies assess only isolated configurations (PV or BSS), short horizons, and limited operational realism. For decision-makers, this hinders both operational choices (industrial daily scheduling, asset dispatch) and strategic ones (sizing PV/BSS, participation in flexibility markets) [9].

This paper develops and validates a time-varying tariff-based scheduling framework that explicitly coordinates PV and BSS with the grid, and exports market-ready APPs. Each APP is tagged with an activation cost and feasibility safeguards, and is transmitted to an industrial cluster, which serves as an aggregator. Within this cluster, flexible demand from multiple industrial facilities is jointly managed and aggregated for energy system operation and market participation as shown in Figure 1. The framework is validated over multiple 7-day horizons across seasons and production volumes, with and without BSS, reflecting typical planning cycles and seasonal PV/price patterns. Performance is quantified using three key performance indicators (KPIs) aligned to industrial and market objectives: average daily energy-cost reduction versus the current plan (%), CO_2 impact using consumption-based hourly grid factors (%), and average daily flexibility (kWh/day) offered to the cluster. The proposed approach provides a realistic and market-aligned pathway to transform plant-level optimization into deployable and monetizable energy flexibility. This work has been carried out within the FLEX4FACT European research project [10].

The remainder of the paper is organized as follows: Section 2 reviews related literature and positions the contributions. Section 3 details the mathematical methodology and model formulation. Section 4 presents the industrial context, simulation framework as well as results and interpretations. Section 5 concludes and outlines future work.

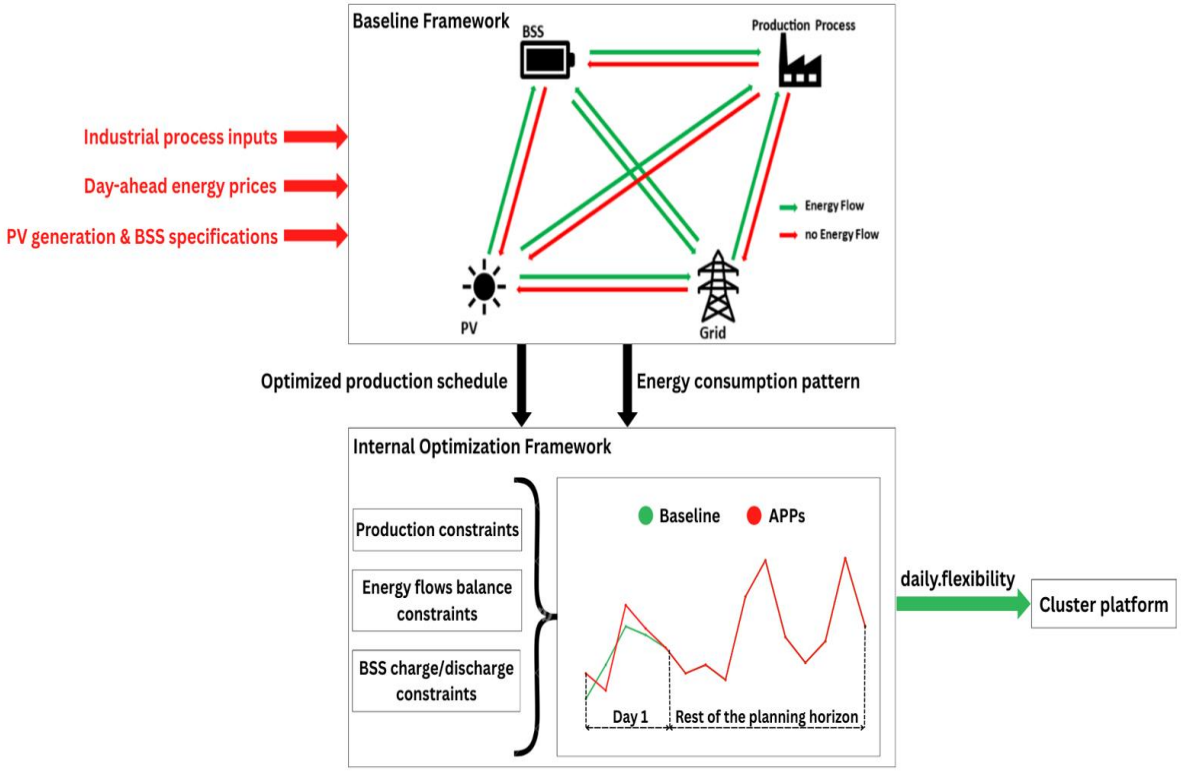

Figure 1: Energy-Flex Model concept and input/output interactions

2 Literature review

This section reviews prior research on energy-aware production scheduling with emphasis on mathematical optimization models, demand-response participation, and the integration of distributed energy resources. It highlights how time-varying electricity pricing and PV/BSS coordination has advanced cost-efficient and flexible industrial operations, while also revealing gaps related to market-ready outputs, longer planning horizons, and realistic plant constraints that motivate the present study.

2.1 Integration of market demand response

Aligning production with time-varying electricity prices is a primary lever to cut cost while supporting decarbonization. Most studies adopt TOU tariffs while a smaller and emerging research engages RTP. Across TOU and RTP studies, the main approach is to reschedule power intensive tasks away from high-price hours with reducing industrial process output, and more recently to account for uncertainty and practical constraints to keep plans feasible.

Under TOU, Park & Ham [11] and Rui et al. [12] demonstrate consistent savings through feasible rescheduling of energy intensive tasks without throughput loss. Wang et al. [13] confirm that price-aware scheduling remains effective under different production constraints (order sizes and storage limits) by analyzing multiple pricing schemes. Extensions to labor limits and preventive maintenance in hybrid flow shops confirm that TOU shifting can be done while respecting staffing and maintenance calendars [14] [15]. For batch processes, Santecchia et al. [16] treat flexible batch units as **"**equivalent batteries**,"** storing low-cost energy in by-products and using corrective scheduling to cushion unplanned shortages.

Moving beyond TOU, a second stream addresses RTP and market participation. Two-stage and stochastic mixed integer linear programming (MILP) formulations co-optimize day-ahead schedules with intraday recourse under different prices scenarios, revealing trade-offs between expected cost reduction and risk exposure [17]. Jabeur et al. [18] jointly schedule a multi-product production plan with on-site renewables, demand-response (DR) participation, inventory/backorder decisions, and emissions constraints. Their results show that synchronizing production with renewable availability and price signals lowers energy cost and carbon impact without degrading service levels.

In summary, RTP-based models appear less frequently compared to TOU. These models also rarely include market offer details like offered energy flexibility and its activation cost, which makes results hard to monetize. Finally, RTP studies often analyses over short horizons, overlooking weekly/seasonal price spreads. In response, the proposed study adopts a scheduling model that evaluates multiple 7-day and seasonal scenarios. Furthermore, it outputs APPs suitable for settlement and reports comparable KPIs (cost, CO_2 using hourly grid factors, and offered flexibility).

2.2 Energy-aware scheduling models

A large share of the literature augments production scheduling with distributed energy resources (DERs), either by adding a single lever (renewables or storage) or by integrating both.

In flow-shop settings, Zhai et al. [19] and Biel et al. [20] integrate wind generation into price-aware flow-shop scheduling, demonstrating that aligning energy-intensive operations with low-price periods and local generation reduces electricity cost, while renewable variability and tighter throughput objectives introduce cost performance trade-offs. On the storage side, Mikhaylidi et al. [21] study a single-machine problem with TOU, introducing a BSS and lateness penalties. The model exploits off-peak charging and on-peak discharging for arbitrage, while the lateness term limits schedule slippage so cost reductions are achieved without unacceptable delivery delays.

Beyond single levers, recent work jointly schedules production with PV and BSS. Liu [22] presents a single-machine model that minimizes total weighted flow time and CO_2 emissions, using Pareto analysis to capture the impact of renewable uncertainty. Zhang et al. [23] formulate a flow-shop model under RTP, showing that jointly optimizing PV self-consumption and battery arbitrage lowers electricity cost compared with PV-only or storage-only strategies. For more complex environments, Moon & Park [24] study a flexible job-shop with integrated PV and BSS, showing that exploiting real-time price volatility yields additional cost reductions while respecting routing and capacity constraints.

Most existing studies examine renewables or storage in isolation, consider only single configurations, or rely on short horizons, which limits comparability across PV–BSS systems and seasonal conditions. In addition, realistic industrial constraints such as shift plans, operating modes, and labor or facility costs are seldom modeled jointly, and market-oriented outputs such APPs with activation costs remain largely unexplored. To address these gaps, this work proposes a tractable framework that co-optimizes production, PV, and BSS across multi-day (7-day) seasonal scenarios and exports APPs for coordinated flexibility provision within an industrial cluster.

3 Mathematical Modelling

The scheduling problem is formulated as a mixed-integer quadratically constrained program (MIQCP). MILPs are widely used in energy aware production scheduling because they allow detailed representation of industrial operating constraints, including equipment interactions and shift-plan limitations [13] [25]. More recent work has also highlighted the importance of linking executable plant schedules with market-oriented energy decisions [26].

Building on these established approaches, the present framework extends the formulation by incorporating quadratic relationships arising from battery storage operation and coupled energy-flow constraints, resulting in a tractable MIQCP model.

The formulation below represents a compact reformulation of the full model used for computation, where the objective functions and most important constraints are included. Different energy flow variants and auxiliary cost constraints, as well as repeated piece-wise relationships are summarized conceptually and provided in the Appendix. The purpose is therefore not to reproduce the entire model in detail, but to highlight the key modeling ideas that drive feasibility and cost performance.

The model consists of two sequential optimization stages. It is designed to quantify the technical and economic benefits of industrial flexibility by jointly optimizing production schedules, PV generation and BSS operation under RTP tariffs:

- **Baseline scheduling:** This generates an executable hourly production plan over a 7-day planning horizon while minimizing total operating cost.
- **Internal optimization:** This produces a set of APPs by advancing or delaying production within the first 24 timesteps of the horizon, while preserving feasibility and maintaining the baseline schedule for the remaining days.

3.1 Baseline Model

The objective function in equation (1) minimizes the total daily cost composed of three elements: the cost of electricity purchased from the grid $E_t^{grid,in}$ in each timestep t, the remuneration earned from PV feed-in $E_t^{grid,out}$, and the auxiliary costs $Aux\_Costs_{l,t}^{op}$ associated with labor and lighting costs:

$$\min\left\{ \sum_{t \in T} \mathrm{E}_{\mathrm{t}}^{\mathrm{grid,in}} \cdot \mathrm{C}_{\mathrm{t}}^{\mathrm{da}} + \sum_{l \in L} \sum_{t \in T} \mathrm{Aux\_Costs}_{\mathrm{l,t}}^{\mathrm{op}} - \sum_{t \in T} \mathrm{E}_{\mathrm{t}}^{\mathrm{grid,out}} \cdot \ \mathrm{rem}^{\mathrm{pv}} \right\} \quad (1)$$

where T and L are the total number of timesteps of the planning horizon and production lines, respectively. C_t^{da} and rem^{pv} are the day-ahead electricity prices on the spot market and the renumeration of PV power feed into the grid, respectively.

To represent the operating limits of the BSS, the charging power is approximated by a piece-wise linear (PWL) function that depends on the state of charge SOC_t at each time t. Constraints (2) and (3) are formulated using a standard Big-M approach, where a sufficiently large constant M is applied to enforce logical conditions in a linear optimization model. Here, they link SOC_t with the PWL indicator variable $pwl_{ind_{c,t}^{ch}}$, ensuring that the corresponding charging-power segment associated with $SOC_{P_c^{ch}}$ can only be activated when the SOC satisfies the required condition. A specific mode of the charging power $pwl_{mode_{c,t}^{ch}}$ can only be active if the battery is charging (both BSS status of charging s_t^{ch} and $pwl_{ind_{c,t}^{ch}}$ are active) as stated in equations (4a) and (4b). The energy flow for charging the BSS $E_t^{bss,in}$ is then restricted using the Big-M approach according to equation (5).

$$SOC_t \leq SOC_{P_c^{ch}} + M \cdot \left(1 - pwl_{ind_{c,t}^{ch}}\right) \ \forall c \in C, t \in T \quad (2)$$

$$SOC_t \geq SOC_{P_c^{ch}} + M \cdot pwl_{ind_{c,t}^{ch}} \ \forall c \in C, t \in T \quad (3)$$

$$pwl_{mode_{c,t}^{ch}} \leq s_t^{ch} \ \forall c \in C, t \in T \quad (4a)$$

$$pwl_{mode_{c,t}^{ch}} \leq pwl_{ind_{c,t}^{ch}} \ \forall c \in C, t \in T \quad (4b)$$

$$E_t^{bss,in} \leq P_c^{ch} + M \cdot \left(1 - pwl_{mode_{c,t}^{ch}}\right) \ \forall c \in C, t \in T \quad (5)$$

*w*here P_c^{ch} is the maximum charging capacity.

Similar constraints define the PWL structure for discharging and impose lower and upper bounds on the state of charge to prevent infeasible battery in the Appendix.

Per time step, the BSS can only charge (BSS charging status $s_t^{ch} = 1$) or discharge (BSS discharging status $s_t^{dch} = 1$) as shown in equation (6). Moreover, equation (7) restricts the change of SOC_t from two consecutive time steps according to the incoming or out-streaming

energy flows minus the natural self-discharging processes Γ of the BSS besides the active charging or discharging.

$$\mathrm{s_t^{ch}} + \mathrm{s_t^{dch}} \leq 1 \;\; \forall \mathrm{t} \in T \tag{6}$$

$$\mathrm{SOC_t} = \mathrm{SOC_{t-1}} \cdot (1 - \Gamma) + \mathrm{E_t^{bss,eff-in}} - \mathrm{E_t^{bss,eff-out}} \;\; \forall \mathrm{t} = 1, \ldots, \mathrm{T} - 1 \tag{7}$$

The equations below formulate the energy-flow constraints linking production demand $E_t^{prod,in}$ to energy supplied by PV generation $E_t^{pv,prod}$, the battery storage system $E_t^{bss,prod}$, and the grid $E_t^{grid,prod}$. They further enforce consistency between hourly production levels and line-specific energy use under technical and operational constraints. The logical links between production decisions, shift-plan variables, and line availability, as well as the constraints associated with auxiliary costs, are reported in the Appendix.

The hourly sum of the energy must match the incoming energy flow into the production facility as shown in equation (8). By assuming that production lines are identical, $E_t^{prod,in}$ is the sum of the consumed energy of the different production lines $E_{l,t}^{prod}$. That is stated in equation (9).

$$E_t^{grid,prod} + E_t^{pv,prod} + E_t^{bss,prod} = E_t^{prod,in} \;\; \forall t \in T \tag{8}$$

$$\sum_{l \in L} E_{l,t}^{prod} = E_t^{prod,in} \;\; \forall t \in T \tag{9}$$

Equation (10) defines the consumed energy as a function of the different technical and operational capacities for each production line:

$$E_{t,l}^{prod} = \left(Prod\_ind_t \cdot \left(E_{t,l}^{prod_{units}} + E^{Shsby\_ind}\right) + ShSby\_ind_t \cdot E^{Shsby\_ind} + LgSby\_ind_t \cdot E^{Lhsby\_ind}\right) \cdot AVAILABILITY_{l,t} + \left(1 - AVAILABILITY_{l,t}\right) \cdot E^{Lgsby_{ind}} \;\; \forall l \in L, t \in T \tag{10}$$

where $Prod\_ind_t$ is the production status. E^{Lgsby_ind} and E^{Shsby_ind} are long and short standby energy consumption per production line, respectively. $AVAILABILITY_{l,t}$ indicates the production line availability (i.e. $AVAILABILITY_{l,t} = 1$ in case of no maintenance).

3.2 Internal optimization model

Equation (11) defines the objective function of the internal optimization. It evaluates the total cost of each APP for each timestep *t* by summing up grid-purchase costs $E_t^{grid,in,APPi} \cdot C_t^{da}$ and auxiliary process costs $Aux_{Costs_{l,T}}^{op,APPi}$, and subtracting revenues from electricity exported to the grid $E_t^{grid,out,APPi}.rem^{pv}$.

$$min\left\{\sum_{t \in T} E_t^{grid,in,APPi} \cdot C_t^{da} + \sum_{l \in L}\sum_{t \in T} Aux_{Costs_{l,T}}^{op,APPi} - \sum_{t \in T} E_t^{grid,out,APPi} \cdot rem^{pv}\right\} \;\; \forall APPi \in N, APPi \in U \tag{11}$$

The rescheduling of the production in the day ahead for APPs is bound to the produced units for each production line obtained in the baseline solution as shown in equation (12).

$$\sum_{l \in L} \sum_{t \in [1,T^{24}]} N_{j,t,l}^{IntOptUnits} = \sum_{l \in L} \sum_{t \in [1,T^{24}]} N_{t,l}^{BaselineUnits} \quad \forall j \in N \tag{12}$$

where $N_{j,t,l}^{IntOptUnits}$ and $N_{t,l}^{BaselineUnits}$ are the hourly produced units per production line for each APP and for the baseline solution, respectively. N is the total number of APPs.

To ensure that the internal optimization only modifies the schedule within the day-ahead window, all baseline-dependent variables and operating constraints are fixed to the values obtained from the baseline solution for the remaining timesteps. In this way, APPs differ only in the first 24 timesteps, while production targets, storage states, and operational feasibility beyond the day-ahead horizon remain identical to the baseline.

To avoid generating identical or dominated solutions, the APPs are ordered according to their total cost. Let CT^{APPi} denote the total cost for each $APPi$, and let CT^{Base} denote the total cost of the baseline. Constraints (13) and (14) ensure that each generated APP has a strictly higher total cost than the previously obtained solution, thereby preventing repetition.

$$CT^{APPi} > CT^{APPi-1} \; \forall \; APPi \in [2, N] \tag{13}$$

$$CT^{1} > CT^{Base} \quad APPi = 1 \tag{14}$$

3.3 KPI formulation

To evaluate the effectiveness of the proposed scheduling framework, a set of KPIs is defined to compare the optimized baseline and APPs with the current industrial practice using consistent energy and emission metrics.

- Average energy flexibility offered per day (kWh/day)

This KPI reports, for each day, the maximum flexibility among all APPs and expresses the sum of obtained flexibility in equation (15) over the first 24 timesteps of the planning horizon T^{24}.

$$KPI_{DailyFlex} = \max_{i \in I} \sum_{t=1}^{T^{24}} |Dailyflex_i(t)| \tag{15}$$

where I is the total number of APPs and $Dailyflex_i(t)$ is defined as the difference between its energy-consumption profile and that of the baseline.

- Average reduction of daily energy cost (%)

This indicator quantifies the economic benefit of the optimized baseline schedule relative to the current production planning. It compares the daily electricity cost of the as-is plan $Cost_{asis}$ with the cost of the baseline obtained from the optimization $Cost_{baseline}$ and expresses the relative reduction.

$$KPI_{EnCost} = \frac{Cost_{asis} - Cost_{baseline}}{Cost_{asis}} \cdot 100 \tag{16}$$

- Industry emissions decrease (%)

Environmental performance is assessed by comparing the CO_2-equivalent emissions of the optimized baseline $CO2_{baseline}$ with those of the current schedule $CO2_{asis}$. Emissions are calculated using hourly grid emission factors, and the KPI expresses the percentage reduction achieved through optimized scheduling.

$$KPI_{Emissions} = \frac{CO2_{asis} - CO2_{baseline}}{CO2_{asis}} \quad (17)$$

4 Simulation framework and results

This section presents the simulation setup and validation results of the proposed Energy-Flex scheduling framework. The model is evaluated using real industrial data across multiple 7-day planning horizons representing different seasonal and production-volume conditions. KPIs on energy cost, CO_2 emissions, and offered flexibility are reported and discussed for scenarios with and without battery storage.

4.1 Simulation framework

The proposed Energy-Flex scheduling framework is validated using a real-world industrial case study from the electronics manufacturing sector. The facility consists of multiple soldering lines, associated assembly units, and intermediate buffer areas that together form complete production lines. Soldering operations represent the dominant electricity consumers and can be executed in either continuous or batch mode. To ensure product quality and avoid excessive thermal cycling, production lines may operate in standby mode to maintain solder temperature or be fully shut down when feasible. These operating-state dependencies create strong interrelations between production feasibility and energy-aware scheduling decisions.

To evaluate performance under representative seasonal and operational conditions, simulations are conducted across six historical 7-day horizons between January and June 2025. These periods include two weeks per season (winter, spring/autumn, summer), each covering one high-production and one low-production order volume week. The selected start dates are 06/01, 27/01, 07/04, 28/04, 19/05, and 23/06. Each scenario is evaluated under multiple BSS sizing configurations, including a no-storage reference case, reflecting typical planning cycles and seasonal variations in PV availability and electricity price spreads.

The industrial site is modelled with rooftop PV generation of 116 kW peak capacity and an average daily electricity demand of several thousand kWh. Since detailed measurements are available for only one production line, all modeled production lines are assumed to share identical technical characteristics. This enables consistent scaling of per-unit energy use, standby behavior, and auxiliary cost assumptions across the plant.

The simulation relies on real-world input data from the following sources:

- **Hourly day-ahead electricity prices**: Hourly German day-ahead market prices for the period January–June 2025, obtained from the SMARD platform [27].
- **CO_2-equivalent factors**: Hourly grid emission factors derived from the CO2Map platform and correlated with the simulated scenarios [28].
- **PV generation**: Hourly PV generation profiles provided by an energy digital twin developed for the factory case study within the FLEX4FACT research project.
- **Per-unit energy use**: The consumed energy per produced unit is estimated by correlating historical energy consumption data with production order plans for each planning horizon.

To ensure comparability between historical and optimized schedules, a coherent synthetic hourly consumption profile is constructed from metered trends and applied consistently to both the baseline and optimized results. This approach enables robust and comparable KPI estimation for energy cost, PV self-consumption, and CO_2 emissions.

The performance of the proposed flexibility algorithms is assessed using the three KPIs defined in Section 3.3. Results are reported for each simulated week without battery storage and with different battery sizes, and seasonal as well as order-volume variations are aggregated into overall averages. Before the start of the project, target values for the three KPIs were defined. These are highlighted in Table 1 with the validation aiming to achieve a 5–10% reduction in total energy consumption and to increase PV self-consumption from around 15% to 25% while maintaining throughput and product quality.

Table 1: KPI overview and target values

KPI #	KPI name	Target Value
$KPI_{DailyFlex}$	Average Energy flexibility offered per day (by the factory to the cluster)	+/- 30 kWh/day
KPI_{EnCost}	Average reduction of daily energy cost with the optimized production	>5%
$KPI_{Emissions}$	Industry emissions decrease with respect to current production	>5%

4.2 Results and interpretations

Simulations were performed with the PV system described above and various BSS configurations. The initial results shown below refer to the case in which only the PV system without BSS was considered.

Figure 2 summarizes all three KPI results across the simulated planning horizons, covering different seasons and both high- and low-order production weeks. Energy cost savings KPI_{EnCost} (Figure 2-a) are strong in no-BSS scenarios, indicating stronger dependence on price patterns and PV availability.

CO_2 emissions, which are represented by $KPI_{Emissions}$, shown in Figure 2-b, behave differently than the costs. The optimized schedules generally reduce CO_2 compared to the as-is case, which is consistent with shifting load toward hours of lower electricity prices and higher PV penetration, because typically these hours have lower emission factors. However, this is not always the case. For instance, in the simulation week starting on 23/06, there is a significant cost decrease and almost no emission decrease. This is because hours with low prices can sometimes have comparatively higher emission factors. Therefore, although the total costs decrease, CO_2 emissions do not always decrease to the same extent.

Flexibility $KPI_{DailyFlex}$ in Figure 2-c consistently exceeds target levels in all scenarios, reaching an average value of 147.34 kWh/day. However, for the planning horizon starting 06/01**,** Figure 2-c shows no flexibility offered because internal optimization only generates APPs by shifting production within the day-ahead window (first 24 timesteps) while keeping scheduling for the rest of the planning horizon equal to the baseline. In this case, with nothing to shift, no APPs can be generated, so no flexibility is available.

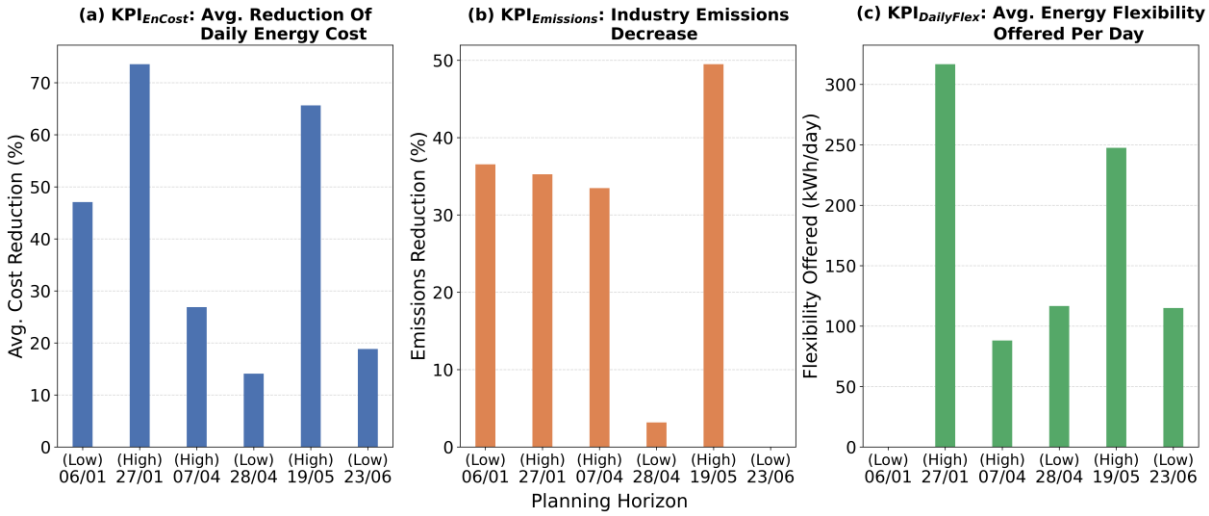

Figure 2: Seasonal and production-volume dependence of energy cost, CO_2 reduction, and offered daily flexibility KPIs

In the following, different BSS configurations were added to the PV. Figure 3 shows the values of KPI_{EnCost} for the simulated planning horizons, comparing seasonal conditions, production volumes, and different battery storage sizes. The results in Figure 3 show a clear seasonal effect on the value of storage. In winter weeks, the highest cost reductions are achieved with small BSS capacities, while increasing storage size does not improve savings and can even reduce them. From spring on, the benefit grows significantly: in the 07/04 scenario savings increase from 52% at 50 kWh to 63% at 288 kWh, and in the low-order production week of 28/04 they rise from 17% at 100 kWh to over 70% at 600 kWh. Larger storage is therefore most effective when PV generation is high and production demand is low, allowing more PV energy to be stored and shifted to high-price hours. Beyond roughly 350 kWh, additional BSS capacity yields only limited additional savings.

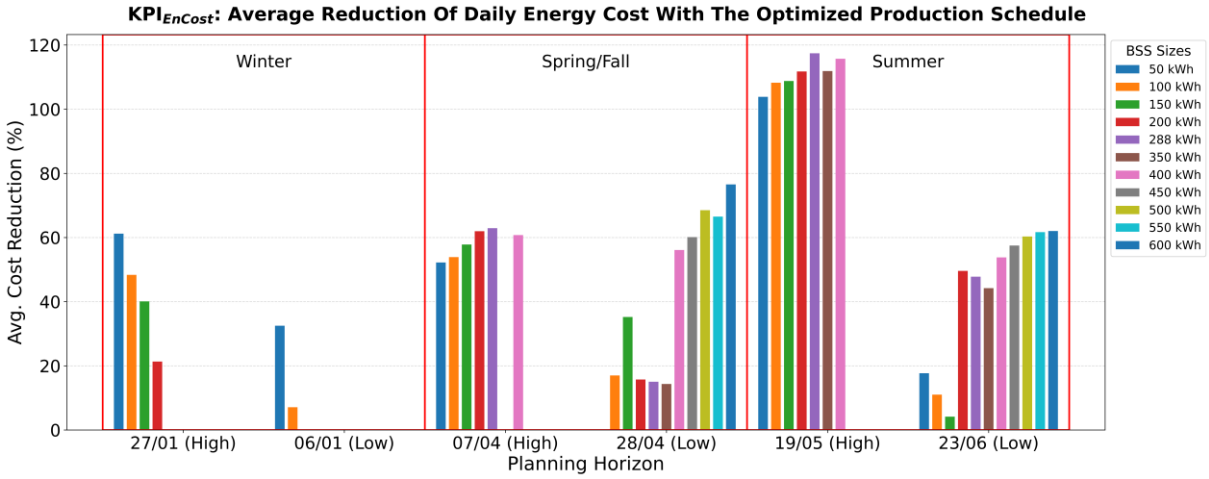

Figure 3: KPI_{EnCost} Average reduction of daily energy cost with the optimized production scheduling for different BSS sizes

Figure 4 presents $KPI_{Emissions}$ values across different seasons, high- and low-order production weeks, and BSS capacities. The results show that CO_2 performance is strongly dependent on storage size and season. The largest emission reductions occur with small BSS capacities

(50–150 kWh), where reductions reach 75.7% on 07/04 and 69.7% on 19/05. As storage size increases, the benefit declines sharply. In the same planning week (19/05), the reduction falls to 4% at 200 kWh and becomes 0% for capacities ≥288 kWh. A similar pattern is observed in winter, where reductions drop from 31.5% at 50 kWh to 0% from 150 kWh. In some horizons, such as 28/04, no CO_2 improvement is obtained for any BSS size. These results indicate that larger storage does not automatically improve emissions. Once the battery begins charging more frequently during hours with higher grid carbon intensity, the CO_2 benefit is neutralized. It should be noted that KPI values reported as 0% do not necessarily imply unchanged emissions. In some cases, the optimized operation leads to even higher CO_2 emissions, but negative reductions are not displayed and are therefore truncated to zero in the results. The environmental value of storage therefore depends primarily on charging from PV surplus rather than from the grid.

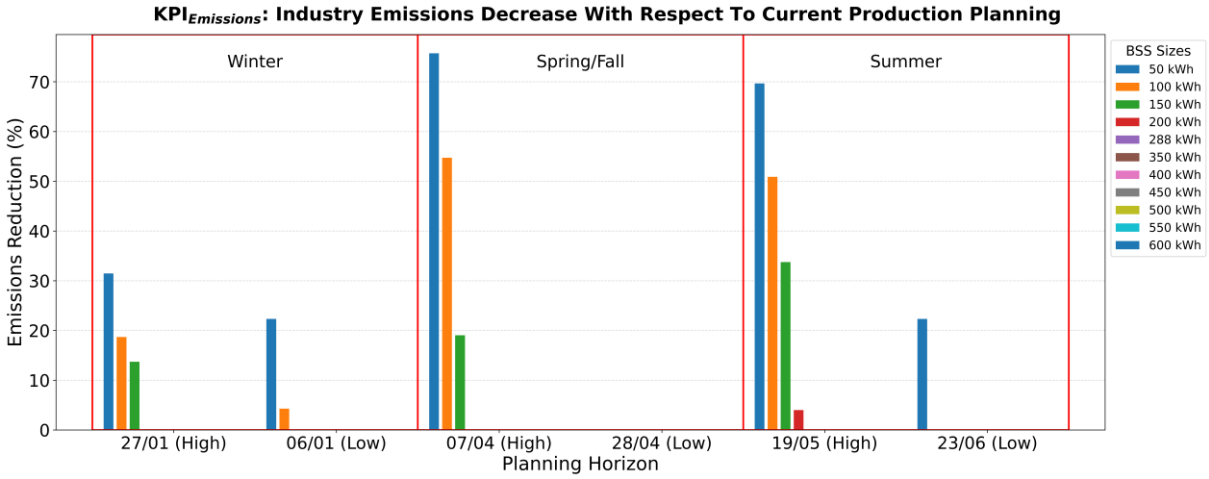

Figure 4: $KPI_{Emissions}$ Industry emissions decrease with respect to current production planning for different BSS sizes

Figure 5 presents $KPI_{DailyFlex}$ values across different seasonal conditions, high- and low-order production weeks, and varying BSS capacities. It shows that the amount of daily flexibility offered is clearly enhanced by the presence of storage. In most plotted horizons the BSS substantially increases flexibility compared to the no-storage case. For example, in the planning week 07/04, $KPI_{DailyFlex}$ rises from 88 kWh/day without BSS to 400 kWh/day at 150 kWh for BSS capacity, and in week 23/06 from 115 kWh/day to 460 kWh/day at 350 kWh. The improvement is not linearly dependent of the size. Medium BSS capacities between 200–400 kWh often deliver the highest flexibility, while further enlargement brings little additional benefit.

The sensitivity to BSS size is particularly strong in low-order spring and summer weeks, where more PV surplus is available for shifting into high-value hours. Overall, the results confirm that storage acts as a flexibility multiplier, but the achievable volume is determined by the interaction of PV availability and the baseline production schedule rather than by capacity alone.

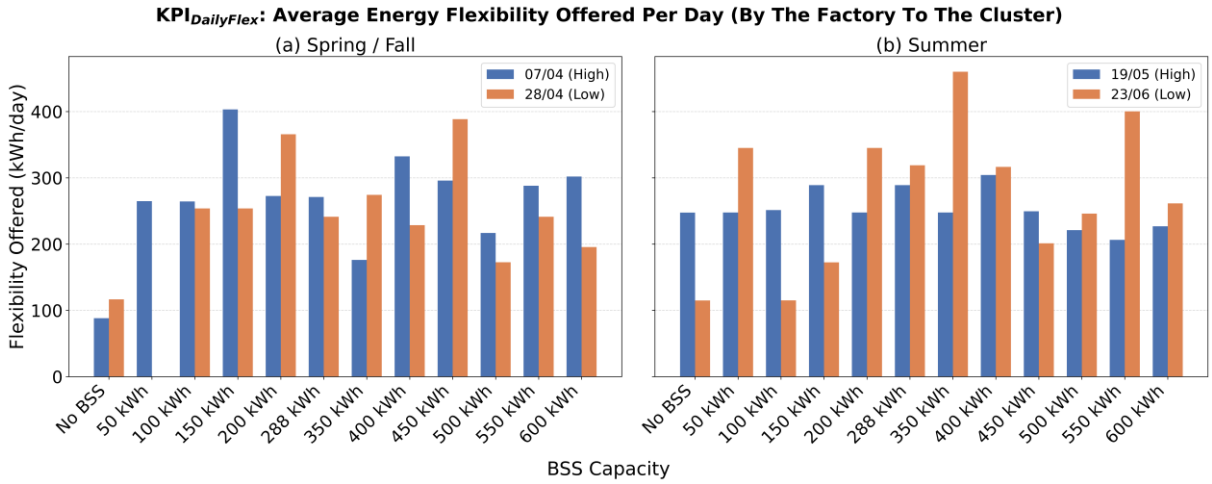

Figure 5: $KPI_{DailyFlex}$ Average energy flexibility offered per day (by the factory to the cluster) for different BSS sizes

5 Conclusion

This paper presents an Energy-Flex scheduling framework that co-optimizes industrial production planning with on-site PV generation and battery storage under time-varying electricity tariffs. The approach produces an executable baseline schedule and alternative production plans with activation costs, enabling coordinated flexibility provision within an industrial cluster. Validation on a real manufacturing case study across multiple 7-day horizons and seasonal conditions confirms that substantial energy-cost reductions are possible while maintaining operational feasibility. Results show that price-aware rescheduling already delivers strong benefits without storage, whereas adding a battery further increases flexibility and cost savings when PV availability and price spreads are favorable. The value of storage is seasonal and non-linear: winter benefits are small, while spring and summer scenarios, especially in weeks with low production orders, show stronger gains, with diminishing returns beyond medium battery sizes. In contrast, CO_2 outcomes do not improve with larger storage capacities under the current charging-hour accounting, indicating that storage does not automatically translate into emission reductions unless charging is aligned with PV surplus or low-carbon hours. Future work will therefore focus on integrating CO_2-aware charging strategies, extending APP generation beyond the day-ahead window, and developing multi-objective formulations that jointly balance cost, flexibility, and emissions to support both operational dispatch and strategic PV–BSS sizing decisions.

6 References

[1] U. Administration, Annual Energy Review, Government Printing Office, 2012.

[2] E. Outlook, International Energy Outlook, 2019.

[3] H. Ritchie, M. Roser und P. Rosado, „CO_2 and Greenhouse Gas Emissions," 2020. [Online]. Available: https://ourworldindata.org/co2-and-greenhouse-gas-emissions.

[4] X. Gong, M. V. d. Wee, T. D. Pessemier, S. Verbrugge, D. Colle, L. Martens und W. Joseph, Energy- and Labor-aware Production Scheduling for Sustainable Manufacturing: A Case Study on Plastic Bottle Manufacturing, Procedia CIRP: 387-392, 2017.

[5] E.-d. Jiang und L. Wang, Multi-objective optimization based on decomposition for flexible job shop scheduling under time-of-use electricity prices, Volume 204, 106177, 2020.

[6] International Renewable Energy Agency (IRENA), *Renewable Energy in Manufacturing A technology roadmap for REmap 2030,* 2014.

[7] G. Zubi, R. Dufo-López, M. Carvalho und G. Pasaoglu, The lithium-ion battery: State of the art and future perspectives, Volume 89, 292-308, 2018.

[8] G. P. Georgiadis, C. N. Dimitriadis und M. C. Georgiadis, *Decarbonizing the Industry Sector: Current Status and Future Opportunities of Energy-Aware Production Scheduling,* 2025.

[9] S. Karimi und S. Kwon, *Comparative analysis of the impact of energy-aware scheduling, renewable energy generation, and battery energy storage on production scheduling,* Department of Systems Science and Industrial Engineering, Binghamton University, Binghamton, New York, 2021.

[10] „Flex4Fact," EU research project, [Online]. Available: https://flex4fact.eu/.

[11] M.-J. Park und A. Ham, „Energy-aware flexible job shop scheduling under time-of-use pricing," *International Journal of Production Economics,* Bd. 248, Nr. 108507, 2022.

[12] Z. Rui, X. Zhang, M. Liu, L. Ling, X. Wang, C. Liu und M. Sun, „Graph reinforcement learning for flexible job shop scheduling under industrial demand response: A production and energy nexus perspective," *Computers & Industrial Engineering,* Bd. 193, Nr. 110325, 2024.

[13] X. Wang, B. Chen, Y. Xiao, S. Liao, X. Ye und J. Bai, „Optimized Scheduling Model Considering the Demand Response and Sequential Requirements of Polysilicon Production," *Energies 2024,* pp. 17, 6048, 2024.

[14] A. Mokhtari-Moghadam, P. Pourhejazy und D. Gupta, „Integrating sustainability into production scheduling in hybrid flow-shop environments," *Environ Sci Pollut Res,* 2023.

[15] X. An, G. Si, T. Xia, D. Wang, E. Pan und L. Xi, „An energy-efficient collaborative strategy of maintenance planning and production scheduling for serial-parallel systems under time-of-use tariffs," *Applied Energy,* Bd. Volume 336, Nr. 120794, 2023.

[16] A. Santecchia, I. Kantor, R. Castro-Amoedo und F. Maréchal, „Industrial Flexibility as Demand Side Response for Electrical Grid Stability," *Frontiers in Energy Research,* Bd. 10, Nr. 831462, 2022.

[17] S. H. Germscheid, F. T. Röben, H. Sun, A. Bardow, A. Mitsos und M. Dahmen, „Demand response scheduling of copper production under short-term electricity price uncertainty," *Computers & Chemical Engineering,* Bd. 178, Nr. 108394, 2023.

[18] M. H. Jabeur, S. Mahjoub und C. Toublanc, „Sustainable Production Scheduling with On-Site Intermittent Renewable Energy and Demand-Side Management: A Feed-Animal Case Study," *Energies 2023,* Bd. 16, Nr. 5433.

[19] Y. Zhai, K. Biel, F. Zhao und J. W. Sutherland, „Dynamic scheduling of a flow shop with on-site wind generation for energy cost reduction under real time electricity pricing," *CIRP Annals,* pp. 41- 44, 2017.

[20] K. Biel, F. Zhao, J. W. Sutherland und C. H. Glock, „Flow shop scheduling with grid-integrated onsite wind power using stochastic MILP," *International Journal of Production Research,* pp. 2076 - 2098, 2018.

[21] Y. Mikhaylidi, H. Naseraldin und L. Yedidsion, „Operations scheduling under electricity time-varying prices," *International Journal of Production Research,* pp. 7136 - 7157, 2015.

[22] C.-H. Liu, „Mathematical programming formulations for single-machine scheduling problems while considering renewable energy uncertainty," *International Journal of Production Research,* pp. 1122 - 1133, 2016.

[23] H. Zhang, J. Cai, K. Fang, F. Zhao und J. W. Sutherland, „Operational optimization of a grid-connected factory with onsite photovoltaic and battery storage systems," *Applied Energy,* pp. 1538 - 1547, 2017.

[24] J.-Y. Moon und J. Park, „Smart production scheduling with time-dependent and machine-dependent electricity cost by considering distributed energy resources and energy storage," *International Journal of Production Research,* Bd. 52, Nr. 13, pp. 3922 - 3939, 2014.

[25] P. Fisco-Compte, M. Juanpera, B. Domenech, R. Pastor, M. Ranaboldo und E. Bullich-Massagué, „Sustainable optimal production scheduling methodology under implicit demand response and carbon policy: A manufacturing industry case study," *Applied Energy,* Bd. 384, Nr. 125403, 2025.

[26] L. Leenders, D. F. Hagedorn, H. Djelassi, A. Bardow und A. Mitsos, „Bilevel optimization for joint scheduling of production and energy systems," *Optimization and Engineering,* Bd. 24, pp. 499-537, 2022.

[27] G. F. N. A. e. m. d. platform, „Smard (Strommarktdaten),“ [Online]. Available: https://www.smard.de/en.

[28] U. o. F. Department of Sustainable Systems Engineering (INATECH), „German emission-data platform,“ [Online]. Available: https://co2map.de.

Appendix

- **PWL constraints for BSS discharging**

The structure of the constraints from (A-1) to (A-4) to restrict the discharging behaviour are similar to the beforehand explained constraints for the charging behaviour.

$$SOC_t \leq SOC_{P_d^{dch}} + M \cdot \left(1 - pwl_{ind_{d,t}^{dch}}\right) \ \forall d \in D, t \in T \quad \text{(A-1)}$$

$$SOC_t \geq SOC_{P_d^{dch}} + M \cdot pwl_{ind_{d,t}^{dch}} \ \forall d \in D, t \in T \quad \text{(A-2)}$$

$$pwl_{mode_{c,t}^{dch}} \leq s_t^{dch} \ \forall c \in C, t \in T \quad \text{(A-3a)}$$

$$pwl_{mode_{c,t}^{dch}} \leq pwl_{ind_{c,t}^{dch}} \ \forall c \in C, t \in T \quad \text{(A-3b)}$$

$$E_t^{bss,out} \leq P_c^{dch} + M \cdot \left(1 - pwl_{mode_{c,t}^{dch}}\right) \ \forall c \in C, t \in T \quad \text{(A-4)}$$

- **Bounds and state constraints of the SOC by the BSS**

Equations (A-5) to (A-7) define the SOC limits of the BSS using the parameters υ^{init}, $\upsilon^{final,lb}$ and $\upsilon^{final,ub}$, which represent the initial SOC and the lower and upper bounds of the final SOC as fractions of the maximum capacity υ^{max}. Constraint (A-5) sets the initial SOC at $t = 0$, while constraint (A-6) enforces that the SOC at the end of the horizon remains within the specified final bounds. Constraint (A-7) links the SOC-dependent piecewise-linear discharging modes to the binary discharging status.

$$SOC_t = \upsilon^{init} \cdot \upsilon^{max} + E_t^{bss,eff-in} - E_t^{bss,eff-out} \ \forall t = 0 \quad \text{(A-5)}$$

$$\upsilon^{final,lb} \cdot \upsilon^{max} \leq SOC_t \leq \upsilon^{final,ub} \cdot \upsilon^{max} \ \forall t = T - 1 \quad \text{(A-6)}$$

$$pwl_{ind_{d,t}^{dch}} + s_t^{dch} = 2 \Rightarrow pwl_{mode_{d,t}^{dch}} = 1 \ \forall t \in T \quad \text{(A-7)}$$

where $E_t^{bss,eff-in}$ and $E_t^{bss,eff-out}$ are the effective energy flow into and from the BSS, respectively.

Equations (A-8)–(A-13) describe the energy inflow and outflow of the BSS. Equation (A-8) links the battery outflow $E_t^{bss,out}$ directly to the energy supplied to the production facility $E_t^{bss,prod}$. Equation (A-9) defines the battery inflow $E_t^{bss,in}$ as the sum of charging energy coming from the grid $E_t^{grid,bss}$ and from PV generation $E_t^{pv,bss}$. The binary variables s_t^{dch} and s_t^{ch} enforce mode-dependent operation: when discharging is active, $E_t^{bss,prod}$ must be positive (equation (A-10)), and when charging is active, energy must flow into the battery from either the grid or PV (equation (A-11)). Conversely, if discharging or charging is inactive, the corresponding energy flows rare forced to zero as stated in equations (A-12) and (A-13).

$$E_t^{bss,prod} = E_t^{bss,out} \ \forall t \in T \quad \text{(A-8)}$$

$$E_t^{grid,bss} + E_t^{pv,bss} = E_t^{bss,in} \ \forall t \in T \quad \text{(A-9)}$$

$$s_t^{dch} = 1 \Longrightarrow E_t^{bss,prod} > 0 \ \forall t \in T \quad \text{(A-10)}$$

$$s_t^{ch} = 1 \Longrightarrow E_t^{grid,bss} + E_t^{pv,bss} > 0 \ \forall t \in T \quad \text{(A-11)}$$

$$s_t^{dch} = 0 \Longrightarrow E_t^{bss,prod} = 0 \ \ \forall t \in T \tag{A-12}$$

$$s_t^{ch} = 0 \Longrightarrow E_t^{grid,bss} + E_t^{pv,bss} = 0 \ \ \forall t \in T \tag{A-13}$$

- **Efficiency constraints for charging & discharging of the BSS**

For numerical reasons of the currently used solver, the division of the energy outflow by the discharging-efficiency-parameter η^{dch} must be accomplished via the helper constraint (A-14) that is then multiplied to consider the efficiency in equation (A-15). This workaround is similar to the formula $\frac{E_t^{bss,out}}{\eta^{dch}} = E_t^{bss,eff-out}$, but can´t be accomplished on this easier way. The charging efficiency is η^{ch} hold by equation (A-16).

$$\eta_t^{aux} \cdot \eta^{dch} = 1 \ \ \forall t \in T \tag{A-14}$$

$$E_t^{bss,out} \cdot \eta_t^{aux} = E_t^{bss,eff-out} \ \ \forall t \in T \tag{A-15}$$

$$E_t^{bss,in} \cdot \eta^{ch} = E_t^{bss,eff-in} \ \ \forall t \in T \tag{A-16}$$

- **Energy flows constraints (PV/Grid)**

Equation (A-17) defines the allocation of on-site PV generation PV_t at each time step. The available PV energy is distributed across three possible flows: energy supplied directly to the production facility $E_t^{pv,prod}$, energy used to charge the battery storage system $E_t^{pv,bss}$, and energy exported to the grid $E_t^{pv,grid}$.

$$E_t^{pv,prod} + E_t^{pv,bss} + E_t^{pv,grid} = PV_t \ \ \forall t \in T \tag{A-17}$$

Constraints (A-18) and (A-19) set the inflow and outflow of energy from and to the grid, that are taken into account in the objective function.

$$E_t^{grid,bss} + E_t^{grid,prod} = E_t^{grid,in} \ \ \forall t \in T \tag{A-18}$$

$$E_t^{pv,grid} = E_t^{grid,out} \ \ \forall t \in T \tag{A-19}$$

- **Shift plan constraints**

sh_s is a binary variable indicating the scheduled production per shift. Equation (A-20) restricts the shift plan input to binary values.

$$sh_s = \begin{cases} 1, \ \text{if Production is scheduled} \\ 0, \ \text{otherwise} \end{cases} \quad \forall s \in S \tag{A-20}$$

Equation (A-21) defines the operating status $\mathrm{prod\_inf}_s$ of the production line based on the shift plan sh_s. On one hand, a production status ("prd") is set when shift plan binary parameter is equal 1. On the other hand, the production line status is characterized by either a short standby ("ssb") or a long standby ("lsb") as follows:

$$prod\_inf_s = \begin{cases} \text{"prd"}, \ \text{if } sh_s = 1 \\ \text{"ssb"}, \text{if } sh_s = 0 \text{ and } sh_{s-1} = 1 \text{ and } sh_{s+1} = 1 \\ \text{"lsb"}, \text{if } sh_s = 0 \text{ and } sh_{s-1} = 1 \text{ and } sh_{s+1} = 0 \\ \text{"lsb"}, \text{if } sh_s = 0 \text{ and } sh_{s-1} = 0 \end{cases} \quad \forall s \in S \tag{A-21}$$

Equations (A-22) to (A-24) transfer the operating status of the production line per shift to binary parameters defined for each time step of the planning horizon. The operating status "prd", "lsb" and "ssb" are assigned to $Prod\_ind_t$, $LgSby\_ind_t$, $ShSby\_ind_t$, respectively.

$$Prod\_ind_t = \begin{cases} 1, & \text{if } prod\_inf_{(t+7)div8} = \text{"prd"} \\ 0, & \text{otherwise} \end{cases} \quad \forall t \in T \tag{A-22}$$

$$LgSby\_ind_t = \begin{cases} 1, & \text{if } prod\_inf_{(t+7)div8} = \text{"lsb"} \\ 0, & \text{otherwise} \end{cases} \quad \forall t \in T \tag{A-23}$$

$$ShSby\_ind_t = \begin{cases} 1, & \text{if } prod_{inf_{(t+7)div8}} = \text{"ssb"} \\ 0, & \text{otherwise} \end{cases} \quad \forall t \in T \tag{A-24}$$

- **Units and production line constraints**

The total number of produced units N^{Units} is hourly distributed over two production lines $N_{t,1}^{Units}$, $N_{t,2}^{Units}$ respectively for line 1 and 2, as follows:

$$N^{Units} = \sum_{t \in T} (N_{t,1}^{Units} + N_{t,2}^{Units}) \ \ \forall t \in T \tag{A-25}$$

The hourly produced units per line $N_{t,l}^{Units}$ cannot exceed the maximal line production capacity $N^{MaxUnits}$ (identically valid for both lines) which is determined from analysing the historical production plan of the use case. Therefore:

$$N_{t,l}^{Units} \leq N^{MaxUnits} \quad \forall l \in L, t \in T \tag{A-26}$$

Hence, the hourly energy consumption per production line $E_{t,l}^{prod\_Units}$ is expressed as a function of the number of produced units $N_{t,l}^{Units}$ and consumed energy per unit $E^{Prod\_per\_Unit}$.

$$E_{t,l}^{prod\_Units} = N_{t,l}^{Units} \cdot E^{Prod\_per\_Unit} \ \ \forall l \in L, t \in T \tag{A-27}$$

The usage of the flexibility and consequently the planned production is not valid if the production line is not available for instance due to maintenance work (constraint (A-28)

$$AVAILABILITY_{l,t} = 0 \Longrightarrow N_{t,l}^{Units} = 0 \ \ \forall l \in L, t \in T \tag{A-28}$$

- **Auxiliary costs constraints**

Industrial auxiliary costs $Aux\_Costs_{l,t}^{op}$ are assumed in the baseline model. This variable includes workers costs $w_{l,t} \cdot Personal_t^{op}$ as well as costs paid by the company to ensure the lighting of the facility $n_{l,t} \cdot Light_l^{op}$. Hence, these auxiliary costs are expressed as follows:

$$Aux\_Costs_{l,t}^{op} = n_{l,t} \cdot Light_l^{op} + w_{l,t} \cdot Personal_t^{op} \ \ \forall l \in L, t \in T \tag{A-29}$$

The personal wages are structured per shift as follows:

- Morning and Afternoon Shifts: $zuschg^{Day}$
- Night shift: $zuschg^{Night}$
- Saturday shift: $zuschg^{Sat}$
- Sunday/holiday shift: $zuschg^{Sun/Hol}$

sh_type_t indicates the type of the shift (week-day/Saturday/Sunday/holiday) which is expressed as follows:

- Weekday shift night: $sh\_type_t = 1$

- Saturday shift: $sh\_type_t = 2$
- Sunday/Holiday shift: $sh\_type_t = 3$
- All other shifts: $sh\_type_t = 0$

Equation (A-30) defines the wage coefficient per shift type:

$$\mathrm{wg_t} = \begin{cases} zuschg^{Night}, & \text{if } sh\_type_t = 1 \\ zuschg^{Sat}, & \text{if } sh\_type_t = 2 \\ zuschg^{Sun/Hol}, & \text{if } sh\_type_t = 3 \\ zuschg^{Day}, & \text{if } sh\_type_t = 0 \end{cases} \quad \forall t \in T \tag{A-30}$$

The shift type sh_type_t will be identified based on the date of the input insertion. In general, this date is always a day before the start of the planning horizon which lead to assign each shift to its corresponding day. Furthermore, the scheduling algorithm will be able to identify the holidays by implementing a 10-year calendar of the European holidays in the database.

The wage cost coefficient showed in constraint (A-31) is equal to 1 if a production is planned for $t \in T$ and 0 otherwise. Furthermore, the workers cost for $t \in T$ in constraint (A-32) is the wage coefficient times the average hourly worker´s production cost.

$$w_{l,t} = \begin{cases} 1, & \text{if } N_{t,l}^{Units} > 0 \; or \; Prod\_ind_t = 1 \\ 0, & \text{otherwise} \end{cases} \quad \forall l \in L, t \in T \tag{A-31}$$

$$Personal_t^{op} = Pr^{Pers\_hour} \cdot wg_t \;\; \forall l \in L, t \in T \tag{A-32}$$

The factory lighting depends on the production process area as well as the availability of the sunlight. Equation (A-33) states that the threshold θ for turning on the factory's lights, is determined by the product of the lighting limit percentage of the factory based on the PV production $PVLIMIT$ and the maximum energy production capacity PV^{Max}.

$$\theta = PVLIMIT \cdot PV^{Max} \tag{A-33}$$

$Prod\_line_{l,t}$ is a binary variable that defines the scheduled production per line, as expressed in constraint (A-34).

$$Prod\_line_{l,t} = \begin{cases} 0, & \text{if } N_{t,l}^{Units} = 0 \\ 1, & \text{otherwise} \end{cases} \quad \forall l \in L, t \in T \tag{A-34}$$

Equations (A-35), (A-36) and (A-37) are the constraints that relate the lightening coefficient $n_{t,l}$ to the availability of the production line $Prod\_line_{l,t}$ and the generated solar energy PV_t compared to the daily threshold θ. Equation (A-35) ensures that $n_{t,l} = 1$ if the production line l is operating at time t. $w_{l,t} = 0$, then $n_{t,l}$ must be 0. Constraint (A-36) estimates that the lighting can only be on ($n_{t,l} = 1$) if the available solar energy is less than the threshold θ. If the solar energy exceeds the threshold θ, thus $n_{t,l}$ becomes 0. Equation (A-37) ensures that the factory's lighting is turned on ($n_{t,l} = 1$) when $w_{l,t} = 1$ and the solar energy generated PV_t is less than the daily threshold θ. Conversely, $w_{l,t} = 0$ or if the solar energy generated PV_t exceeds the threshold θ, the constraint allows the lights to be turned off ($n_{t,l} = 0$).

$$n_{t,l} \leq w_{l,t} \tag{A-35}$$

$$n_{t,l} \leq (PV_t < \theta) \tag{A-36}$$

$$n_{t,l} \geq w_{l,t} + (PV_t < \theta) - 1 \;\; \forall l \in L, t \in T \tag{A-37}$$

The lighting costs per production line $Light_l^{op}$ depends on the average lighting per m^2, $Li^{Average}$ Average light energy consumption per m^2,the industrial area of the production line $Area_l^{prod\_line}$ as well as the electricity prices C_t^{da}.

$$Light_l^{op} = Li^{Average} \cdot Area_l^{prod\_line} \cdot C_t^{da} \quad \forall l \in L, t \in T \tag{A-38}$$